Plant Physiology®

Plant Physiology, 2025, **197**, kiae665
https://doi.org/10.1093/plphys/kiae665
Advance access publication 16 December 2024
Research Article

Rubisco packaging and stoichiometric composition of the native β-carboxysome in *Synechococcus elongatus* PCC7942

Yaqi Sun,[1,‡] Yuewen Sheng,[2,‡] Tao Ni,[3,†,‡] Xingwu Ge,[1] Joscelyn Sarsby,[4] Philip J. Brownridge,[4] Kang Li,[5] Nathan Hardenbrook,[3] Gregory F. Dykes,[1] Nichola Rockliffe,[6] Claire E. Eyers,[4] Peijun Zhang,[2,3,7,*] Lu-Ning Liu[1,5,*]

[1]Department of Biochemistry, Cell and Systems Biology, Institute of Systems, Molecular and Integrative Biology, University of Liverpool, Crown Street, Liverpool L69 7ZB, UK
[2]Diamond Light Source, Harwell Science and Innovation Campus, Didcot OX11 0DE, UK
[3]Division of Structural Biology, Wellcome Trust Centre for Human Genetics, University of Oxford, Oxford OX3 7BN, UK
[4]Centre for Proteome Research, Institute of Systems, Molecular and Integrative Biology, University of Liverpool, Crown Street, Liverpool L69 7ZB, UK
[5]College of Marine Life Sciences, and Frontiers Science Center for Deep Ocean Multispheres and Earth System, Ocean University of China, Qingdao 266003, China
[6]Faculty of Health & Life Sciences, GeneMill, University of Liverpool, Crown Street, Liverpool L69 7ZB, UK
[7]Chinese Academy of Medical Sciences Oxford Institute, University of Oxford, Oxford OX3 7BN, UK
*Author for correspondence: luning.liu@liverpool.ac.uk (L.-N.L.), peijun.zhang@strubi.ox.ac.uk (P.Z.)
[†]Present address: LKS Faculty of Medicine, School of Biomedical Sciences, The University of Hong Kong, Pokfulam, Hong Kong SAR, China
[‡]The authors contribute equally to this work.
The author responsible for distribution of materials integral to the findings presented in this article in accordance with the policy described in the Instructions for Authors (https://academic.oup.com/plphys/pages/General-Instructions) is Lu-Ning Liu.

Abstract

Carboxysomes are anabolic bacterial microcompartments that play an essential role in CO_2 fixation in cyanobacteria. This self-assembling proteinaceous organelle uses a polyhedral shell constructed by hundreds of shell protein paralogs to encapsulate the key CO_2-fixing enzymes Rubisco and carbonic anhydrase. Deciphering the precise arrangement and structural organization of Rubisco enzymes within carboxysomes is crucial for understanding carboxysome formation and overall functionality. Here, we employed cryoelectron tomography and subtomogram averaging to delineate the 3D packaging of Rubiscos within β-carboxysomes in the freshwater cyanobacterium *Synechococcus elongatus* PCC7942 grown under low light. Our results revealed that Rubiscos are arranged in multiple concentric layers parallel to the shell within the β-carboxysome lumen. We also detected Rubisco binding with the scaffolding protein CcmM in β-carboxysomes, which is instrumental for Rubisco encapsulation and β-carboxysome assembly. Using Quantification conCATamer-based quantitative MS, we determined the absolute stoichiometric composition of the entire β-carboxysome. This study provides insights into the assembly principles and structural variation of β-carboxysomes, which will aid in the rational design and repurposing of carboxysome nanostructures for diverse bioengineering applications.

Introduction

Biological CO_2 fixation is an essential process in living organisms that enables the conversion of inorganic CO_2 into organic compounds, supporting the global carbon cycle and sustaining life on Earth. The key CO_2-fixation enzyme, ribulose-1,5-bisphosphate carboxylase/oxygenase (Rubisco), captures and converts inorganic carbon to produce a sugar precursor through the Calvin–Benson–Bassham cycle. However, Rubisco is surprisingly inefficient, making its catalytical reactions the limiting steps in photosynthetic CO_2 fixation. The ineffectiveness of Rubisco originates from its slow catalytic rate and poor capability in discriminating between CO_2 and O_2. To overcome the inherent limitations, distinct organisms, including many bacteria, algae, C_4 plants, and crassulacean acid metabolism plants, have evolved various CO_2-concentrating mechanisms (CCMs) to accumulate CO_2 around Rubisco (Field et al. 1998; McGrath and Long 2014; Gonzalez-Esquer et al. 2016; Long et al. 2016; Rae et al. 2017). In contrast, an overwhelming majority of agricultural crops, namely C_3 plants, lack any form of CCM, resulting in a lower photosynthetic efficiency (Price et al. 2013). Deciphering how the CCM systems work in nature and introducing a functional CCM into crop plants to supercharge CO_2 fixation in C_3 plants and enhance crop yields has received increasing attention.

Carboxysomes are a family of bacterial microcompartments responsible for CO_2 fixation and serve as the central component of CCMs in cyanobacteria and some proteobacteria (Kerfeld and Erbilgin 2015; Liu 2022). The carboxysome sequesters the key CO_2-fixing enzyme, ribulose 1,5-bisphosphate carboxylase/oxygenase (Rubisco), and carbonic anhydrase (CA), using a polyhedral protein shell (Fig. 1A). The carboxysome shell is constructed from multiple protein paralogs (including hexamers, pentamers, and trimers) through self-assembly. Their intrinsic architectural properties enable carboxysomes to play a crucial role in the global carbon cycle and primary productivity (Behrenfeld et al. 2001; Rae et al. 2013; Faulkner et al. 2017; Kerfeld et al. 2018; Sun et al. 2019; Sun et al. 2022). Understanding the assembly and organizational principles of carboxysomes is of key importance not only for elucidating carboxysome function and catalytic performance but also for harnessing their potential in synthetic engineering for various biotechnological applications (Liu 2021; Liu et al. 2021).

There are 2 carboxysome lineages, α-carboxysomes and β-carboxysomes, which differ in the types of encased Rubisco, the composition of building proteins, subcellular distribution, and biogenesis pathway (Price et al. 2008; Rae et al. 2013; Kerfeld and Melnicki 2016). For example, α-carboxysomes encapsulate Form 1A

Received October 4, 2024. Accepted November 22, 2024.
© The Author(s) 2024. Published by Oxford University Press on behalf of American Society of Plant Biologists.
This is an Open Access article distributed under the terms of the Creative Commons Attribution License (https://creativecommons.org/licenses/by/4.0/), which permits unrestricted reuse, distribution, and reproduction in any medium, provided the original work is properly cited.

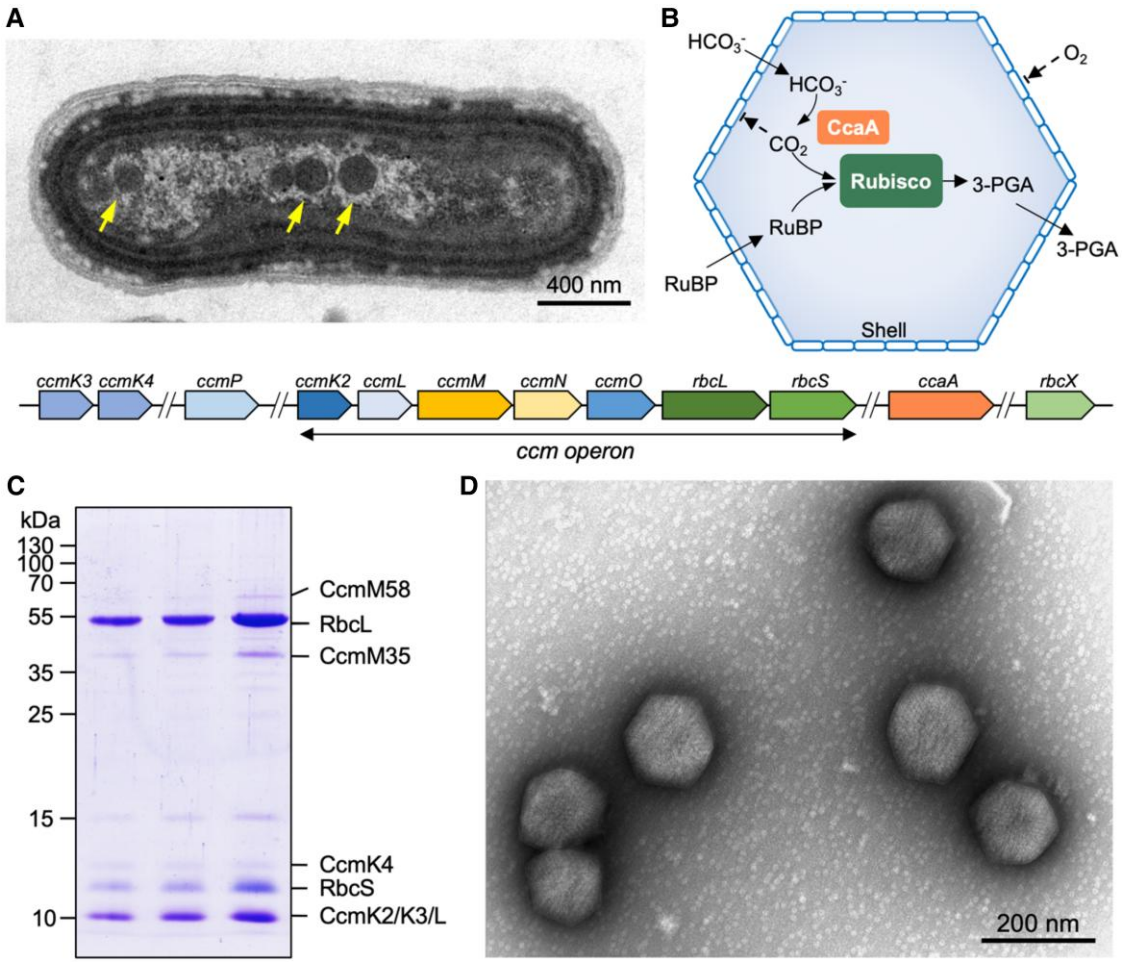

Figure 1. Purification and characterization of Syn7942 β-carboxysomes. **A)** Thin-section electron microscopy of a Syn7942 cell with β-carboxysomes indicated by arrows (top) and the organization of genes expressing β-carboxysome proteins in the Syn7942 genome (bottom), **B)** Functional diagrams of β-carboxysomes. The carboxysome shell is selectively permeable, allowing HCO_3^- and RuBP to enter while blocking O_2 influx and preventing CO_2 leakage to the cytoplasm. Within the β-carboxysome lumen, CcaA catalyzes the dehydration of HCO_3^- to CO_2, providing elevated levels of CO_2 around the Rubisco active sites in the carboxysome lumen to enhance CO_2 fixation, **C)** SDS–PAGE of purified β-carboxysomes from 3 biological replicates. The bands near 15 kDa likely corresponded to egg lysozyme (14.4 kDa) used during purification, as determined previously (Long et al. 2005; Faulkner et al. 2017), and **D)** electron microscopy image of isolated β-carboxysomes from Syn7942.

Rubisco, and their biogenesis may undertake simultaneous and/or independent Rubisco core assembly and shell encapsulation (Iancu et al. 2010); in contrast, β-carboxysomes encapsulate Form 1B Rubisco, exhibit even distribution inside the cells (Savage et al. 2010), and de novo assembly of β-carboxysomes exploits the "inside–out" model (Cameron et al. 2013; Chen et al. 2013). Despite the evolutionary and structural differences, it has been indicated that the diverse Rubisco forms found in α- and β-carboxysomes exhibited similar kinetic parameters, and both types of carboxysomes may possess comparable functional capabilities (Whitehead et al. 2014).

The β-carboxysome of the cyanobacterium *Synechococcus elongatus* PCC7942 (Syn7942) has been extensively characterized as a model carboxysome (Fig. 1B). The cargo enzymes of the Syn7942 β-carboxysome include Form IB Rubisco (comprising Rubisco large and small subunits RbcL and RbcS), which have a higher catalytic rate than that of plant Rubisco (Whitney et al. 2011; Orr et al. 2020), as well as β-CA (also known as CcaA). The shell consists of a series of proteins encoded by the *ccm* operon, including the structural proteins CcmK2, CcmK3, and CcmK4, which appear as hexamers and predominantly form shell facets (Kerfeld et al. 2005), CcmL pentamers that occupy the vertices of the polyhedron (Tanaka et al. 2008), as well as the trimeric proteins CcmO and CcmP (Cai et al. 2013; Larsson et al. 2017). CcmM presents in 2 isoforms, CcmM35 and CcmM58, both of which are essential for β-carboxysome assembly (Long et al. 2007, 2010). While both CcmM35 and CcmM58 act as "linkers" to promote Rubisco nucleation in β-carboxysome biogenesis, CcmM58 binds with CcmN to facilitate shell-interior association (Eisenhut et al. 2007; Long et al. 2007, 2010; Kinney et al. 2012; Gonzalez-Esquer et al. 2015; Ryan et al. 2019; Wang et al. 2019), essential for de novo assembly of β-carboxysomes (Cameron et al. 2013; Chen et al. 2013). Moreover, auxiliary factors Raf1 and RbcX are involved in β-carboxysome formation and regulation. Raf1 mediates the assembly of Rubisco holoenzymes and the biogenesis of intact β-carboxysomes (Huang et al. 2020). RbcX serves as a component of the carboxysome and plays a role in mediating β-carboxysome assembly and subcellular distribution (Huang et al. 2019). In the β-carboxysomes that contain CcmK1, a chaperon protein CcmS has recently been determined to play an important role in mediating β-carboxysome formation through interaction with the CcmK1 C-termini exposing at the outer surface of the shell (Chen et al. 2023; Cheng et al. 2024).

Despite the substantial efforts made over the past decades to understand the functions of individual carboxysome components, the precise composition of carboxysomes and how the building proteins assemble and self-organize to form intact carboxysome structures remain fundamental questions. Recent studies have provided detailed information on the encapsulation and spatial arrangement of Rubiscos within α-carboxysomes (Metskas et al. 2022; Ni et al. 2022a, 2022b; Evans et al. 2023; Ni et al. 2023), as well as the exact protein stoichiometry of α-carboxysomes (Sun et al. 2022). The β-carboxysomes exhibit structural and compositional variations under different environmental conditions; for example, β-carboxysomes can vary in size, with diameters spanning from 144 to 208 nm, depending on the light and CO_2 conditions (Sun et al. 2019). A recent study characterized the Rubisco organization of β-carboxysomes isolated from Syn7942, which have a diameter of 193 nm (Kong et al. 2024). However, how the Rubisco organization is modulated within the β-carboxysomes of varying sizes, as well as the precise composition of intact β-carboxysomes, remains unclear. This knowledge gap is among the major obstacles in the construction of functional intact β-carboxysomes in nonnative organisms for bioengineering applications.

In this study, we isolated intact β-carboxysomes with a reduced diameter of 169 nm from Syn7942 cells that were cultivated under low-light conditions and determined the spatial packaging of Rubisco mediated by CcmM within the smaller β-carboxysome using cryoelectron tomography (cryoET). Moreover, we performed absolute quantification of protein components within the native β-carboxysome using Quantification conCATamer (QconCAT)-assisted quantitative MS in combination with biochemical analysis and enzymatic assays. Our results provide a structural basis for a detailed understanding of the assembly principles and structural regulation of β-carboxysomes. Advanced knowledge of carboxysome assembly and modulation will aid in the rational design and synthetic engineering of carboxysome-based structures.

Results

Structure and assembly of Rubisco in isolated Syn7942 β-carboxysomes

Our previous studies indicated that β-carboxysomes produced under low-light conditions tend to be smaller in diameter and more uniform in shape (Sun et al. 2019), which may make them suitable for in-depth structural and biochemical analysis. Therefore, we purified intact β-carboxysomes from Syn7942 grown under a naturally relevant lower light (15 $\mu E\ m^{-2}\ s^{-1}$) using sucrose gradient ultracentrifugation (Faulkner et al. 2017) (Supplementary Fig. S1A). The β-carboxysome proteins were identified by SDS-polyacrylamide gel electrophoresis (SDS–PAGE) (Fig. 1C) and immunoblot analysis (Supplementary Fig. S1B). Negative-staining electron microscopy (EM) revealed that the isolated β-carboxysomes formed intact polyhedral shapes with clear borders (Fig. 1D). The CO_2-fixation rate of isolated β-carboxysomes was measured as $2.56 \pm 0.16\ \mu mol\ mg^{-1}\ min^{-1}$ ($n = 3$ independent biological samples), which is comparable to that of α-carboxysomes from the chemoautotrophic bacterium *Halothiobacillus neapolitanus*, when tested under the same experimental conditions (Sun et al. 2022). This is consistent with previous findings (Whitehead et al. 2014). These results confirmed the functional and structural integrity of β-carboxysomes isolated from Syn7942.

We performed cryoET and subtomogram averaging (STA) of the isolated β-carboxysomes using emClarity (Himes and Zhang 2018; Ni et al. 2022a, 2022b) (Fig. 2, Supplementary Table S1). The β-carboxysomes exhibited morphological variations with a size of 169.0 ± 11.8 nm (Supplementary Fig. S1C), which falls within the range of the diameters determined within and isolated from Syn7942 cells in previous studies (Faulkner et al. 2017; Sun et al. 2019). Individual Rubiscos inside the β-carboxysomes were readily delineated in the raw tomograms (Fig. 2A, Supplementary Fig. S2, Supplementary Video S1). Template matching and mapping of the position and orientation of individual Rubisco complexes to the original tomograms revealed that Rubiscos had a paracrystalline arrangement within the β-carboxysome lumen, forming 4 to 9 concentric layers (Fig. 2B, Supplementary Fig. S3A). Among the β-carboxysome particles analyzed, 92.4% had 4 to 6 layers of Rubiscos, with 5 layers being the most frequently observed (44.3%, Supplementary Fig. S3A). The pairwise distance between neighboring Rubiscos is 121.9 ± 31.4 Å (Supplementary Fig. S3B), which is comparable to that of α-carboxysomes (128 to 129 Å) (Ni et al. 2022a, 2022b). Our analysis reveals that each β-carboxysome contains $\sim 639 \pm 194$ Rubisco complexes (Fig. 2C). This quantity is remarkably greater than that of the α-carboxysomes from *Cyanobium* 7001, *H. neapolitanus*, and *Prochlorococcus* (Ni et al. 2022a, 2022b; Evans et al. 2023; Zhou et al. 2024). However, the Rubisco content is notably lower than that observed in larger β-carboxysomes with a diameter of 193 nm (Kong et al. 2024). Whether this variation in Rubisco content within distinct β-carboxysomes is attributed to differences in carboxysome diameter, the spacing between Rubisco pairs, or other factors merits further investigation.

As expected, the content of Rubisco per layer and total Rubiscos per β-carboxysome gradually increased as the number of layers increased from the core center to the shell (Supplementary Fig. S3, C and D). Approximately, layers 1 to 6 contain 1, 20, 71, 174, 308, and 407 copies of Rubiscos, respectively (Supplementary Fig. S3C). This leads to ~600 copies of Rubiscos per Syn7942 β-carboxysome, given that the majority of β-carboxysomes contain 5 layers of Rubiscos (Supplementary Fig. S3A). The inner 4 layers are closely packed and relatively ordered; therefore, we only considered the data within the first 2 to 4 layers to establish a model/formula for the number of Rubiscos for each layer. The prediction was based on the radial distances of Rubiscos from the core as well as the sphere surface area formula ($4\pi r^2$). The average distance between 2 Rubisco complexes is ~120 Å (Supplementary Fig. S3B), as is the distance between 2 consecutive layers. When taking layer 4 as the reference to estimate the total number of Rubiscos for layers 2 and 3, we found that the estimated results closely matched the actual numbers (Supplementary Fig. S3C). Accordingly, this allowed us to extrapolate the number of Rubiscos for layers 5 to 9 in a β-carboxysome that has 9 layers (Supplementary Fig. S3D). Moreover, Rubiscos are mostly oriented with their 4-fold axis along the radial direction (90 °) across all layers (Supplementary Fig. S4, A to C). Interestingly, no significant difference in the orientation of Rubisco was observed within the outermost layer compared to the inner layers (Supplementary Fig. S4D). This suggests that the size of the shell/carboxysome does not have a significant effect on the internal Rubisco arrangement, in line with the "Core first" assembly pathway of β-carboxysomes (Cameron et al. 2013). In contrast, a recent study of β-carboxysomes proposed that the Rubiscos at the outermost layer of β-carboxysomes have a more regular arrangement (Kong et al. 2024). This discrepancy might be ascribed to the structural plasticity of the β-carboxysomes formed under different growth conditions (see detailed discussion below).

We further determined the structure of Rubisco within native Syn7942 β-carboxysomes at a resolution of 3.5 Å using STA (Fig. 2D, Supplementary Fig. S2, Supplementary Video S2). The resolved structure of the Rubisco L_8S_8 hexadecamer was oriented along its 4-fold

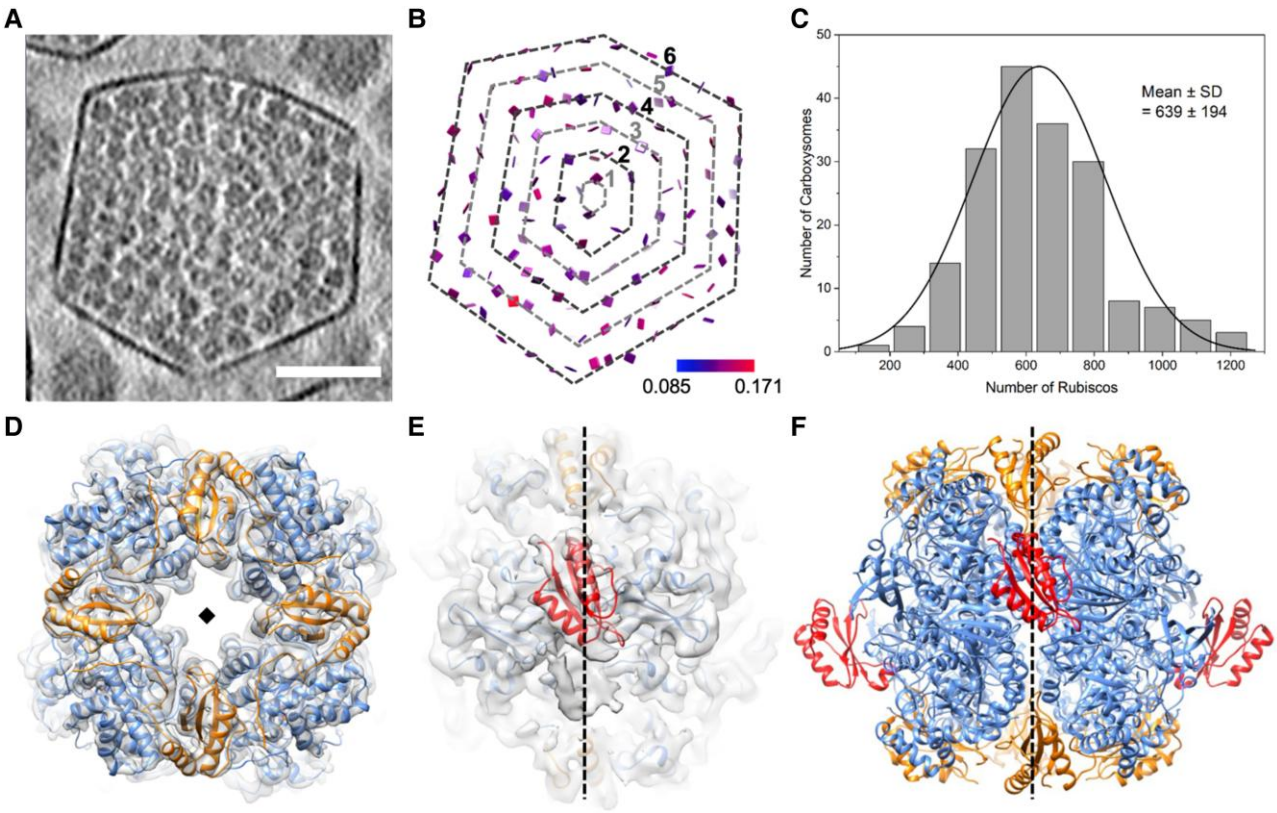

Figure 2. CryoEM structures and organization of Rubisco within β-carboxysomes. **A)** A tomogram slice showing a typical β-carboxysome. Scale bar: 50 nm. **B)** The position and orientation of individual Rubisco mapped back to the tomogram to the tomogram of β-carboxysome in **A)**, shown as a square plate perpendicular to the 4-fold symmetry axis of Rubisco and colored according to the cross-correlation values (0.085 to 0.171, blue to red) between individual Rubisco and the STA map. It contains a total of 6 layers and the layer number is defined from the core to the shell, as shown. **C)** Histogram of Rubisco numbers in β-carboxysomes ($n = 185$). **D)** The cryoET subtomogram averaged structures of Rubisco at 3.5 Å, overlapped with refined atomic model (PDB ID: 8BCM). RbcL subunits are shown in blue and RbcS subunits are shown in orange. **E)** Zoomed-in view showing the density of CcmM, the linker protein which binds Rubisco, fitted with the atomic model of CcmM SSUL (red, PDB ID: 6HBC). CcmM exhibits 2 binding modes (upper groove and lower groove, Supplementary Fig. S5). RbcL subunits are shown in blue and RbcS subunits are shown in orange. **F)** The overall atomic models of Rubisco along with 4 SSUL domains in 2 views. Only one binding mode is shown (upper groove). RbcL, RbcS, and CcmM are shown in blue, orange, and red, respectively. The diamond **(D)** and dashed black lines **(E, F)** indicate the 4-fold axis.

axis along the radial direction, in good agreement with the reported Syn7942 Rubisco structures (Wang et al. 2019; Huang et al. 2020; Kong et al. 2024; Sun et al. 2024). Intriguingly, an extra density in the groove at the interface between antiparallel RbcL dimers was well-resolved (Fig. 2, E and F). This density matches the Rubisco small subunit-like (SSUL) module of the "linker" protein CcmM, which contains 2 α-helices packed against a β-sheet (Fig. 2E). As it sits on the 2-fold axis, the 2-fold symmetrized density appears a half intensity compared to Rubisco, and space can only accommodate 1 module. We thus deduced that one copy of CcmM SSUL can bind to the RbcL groove in either the up or down configuration, but not both (Fig. 2E, Supplementary Fig. S5, Supplementary Video S3). The binding of CcmM SSUL to Rubisco is reminiscent of that of the reconstituted Rubisco–CcmM35 complex [Protein Data Bank (PDB) ID: 6HBC] (Wang et al. 2019). Each Rubisco within the carboxysome has potentially 4 CcmM SSUL domains that can bind Rubisco at the RbcL dimer groove in 2 different modes (Fig. 2, E and F). These cryoET results provide direct evidence of Rubisco–CcmM interactions within β-carboxysomes, which drive the recruitment and packaging of Rubisco to form paracrystalline arrays in the β-carboxysome lumen.

In situ cryoET of β-carboxysomes

We further conducted in situ cryoET to explore the structure of β-carboxysomes in native Syn7942 cells (Fig. 3). The intact β-carboxysome particles exhibit polyhedral shapes and a concentric ring-like arrangement of Rubisco within the carboxysome lumen, corroborating our observations from purified β-carboxysomes (Fig. 2). The observed in vivo structural variability resembles that observed in previous studies of Syn7942 and the findings of α-carboxysomes (Sun et al. 2022). Additionally, β-carboxysomes were located away from the edge of the cell, often accompanied by large electron-dense granules in proximity (Fig. 3, Supplementary Video S4). This likely suggests the physical connections between β-carboxysomes and granules, in line with the observations for α-carboxysomes in *H. neapolitanus* cells (Iancu et al. 2010).

Protein stoichiometry of β-carboxysomes

Owing to the irregular morphology of Syn7942 β-carboxysomes, recognition of additional crucial carboxysome components aside from Rubiscos remains unfeasible via the cryoET approach. Using fluorescence tagging and single-molecule fluorescence microscopy, our previous work has estimated the protein abundance of β-carboxysomes in vivo (Sun et al. 2019). However, given the potential effects of fluorescence tagging and limitations of imaging sensitivity, the precise protein stoichiometry of the β-carboxysome has not been determined. By employing MS-based absolute multiplexed protein quantification using a labeled QconCAT (Rivers et al. 2007; Simpson and Beynon 2012; Johnson et al. 2021), we previously decoded the

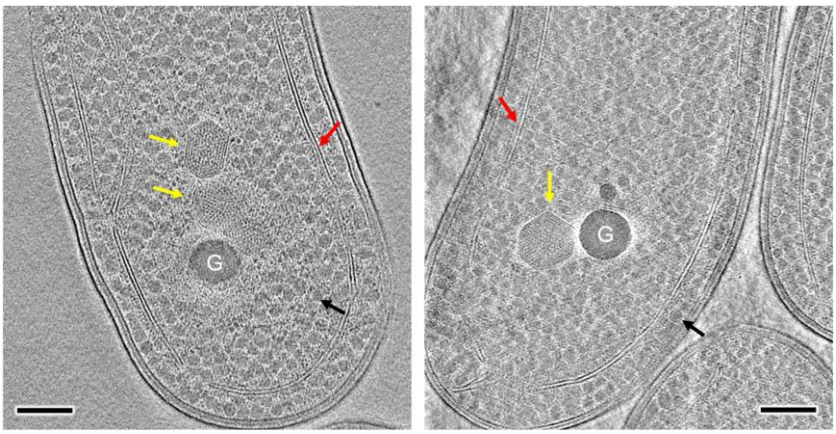

Figure 3. In situ cryoET of frozen-hydrated Syn7942 cell lamella. Yellow arrows indicate the β-carboxysome structures which possess regularly packed Rubisco in the β-carboxysome lumen. G represents large electron-dense polyphosphate granule. Red arrows indicate thylakoid membranes and black arrows indicate glycogen granules. Scale bar, 200 nm. See also Supplementary Video S4.

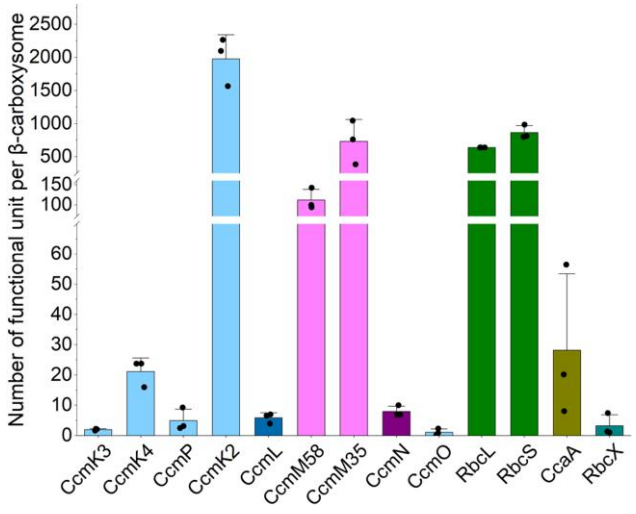

Figure 4. Absolute quantification of the subunit stoichiometry of Syn7942 β-carboxysomes using QconCAT standardization. See also the content of protein oligomers per β-carboxysome in Table 1. Data are presented as means ± SD from 4 independent biological replicates.

accurate stoichiometric composition of protein components of α-carboxysomes and Pdu metabolosomes (Yang et al. 2020; Sun et al. 2022). To establish the stoichiometry of the β-carboxysome components, we employed high-resolution liquid chromatography-MS (LC-MS) with protein-specific stable isotope-labeled internal standards created using the QconCAT approach. This allowed us to determine the absolute stoichiometry of all the protein components in the purified Syn7942 β-carboxysomes (Fig. 4, Table 1). Thus, we provide precise quantification of the protein stoichiometry of the β-carboxysome.

The single QconCAT peptide was designed to contain 2 unique quantification peptides (Q-peptides) for each Syn7942 β-carboxysome protein: CcmK2, CcmK3, CcmK4, CcmL, the CcmM35/58 shared region, CcmM58, CcmN, CcmO, RbcL, RbcS, CcmP, RbcX, and CcaA (Supplementary Fig. S6A, Supplementary Tables S2 and S3). The stable isotope-labeled QconCAT was purified following peptide expression using a cell-free synthesis system (Takemori et al. 2017) (Supplementary Fig. S6B), prior to LC-MS-based absolute protein quantification. To determine the absolute amounts of the β-carboxysome protein components, we prepared fresh isolates and co-digested them with purified isotope-labelled QconCAT. All β-carboxysome proteins were successfully detected (Supplementary Data Set 1), enabling us to determine the abundance of protein components within a single β-carboxysome (Fig. 4, Table 1). This quantification was based on the Rubisco content determined for the β-carboxysome with an average diameter of 169.0 nm, as measured using cryoET (Supplementary Fig. S1C). Our results revealed that the most abundant proteins in the Syn7942 β-carboxysome were CcmK2 hexamers (1,975 copies), followed by Rubisco (639 copies, quantified based on the content of RbcL), CcmM35 (730 copies), CcmM58 (112 copies), β-CA (CcaA) hexamers (McGurn et al. 2016) (28 copies), CcmK4 hexamers (21 copies), CcmP pseudo-hexamers (5 copies), CcmN monomers (8 copies), CcmK3 (2 copies of hexamers, see discussion below), CcmO pseudo-hexamers (1 copy), and RbcX dimers (3 copies). Additionally, 6 copies of CcmL pentamers were detected in the β-carboxysome, which is consistent with previously reported observations (Sun et al. 2019). Overall, the Syn7942 β-carboxysome had a molecular mass of ~529 MDa (Table 1).

In contrast to the low copy numbers of β-CA, Rubisco and CcmK2/K3/K4 hexamers accounted for ~68% and ~25% of the total molecular mass, respectively. The Rubisco-scaffolding protein CcmM has 2 isoforms: a 35-kDa truncated CcmM35 and a full-length 58-kDa CcmM58 (Long et al. 2007; Cot et al. 2008; Long et al. 2010, 2011). CcmM35 contains 3 SSUL domains that interact with Rubisco (Hagen et al. 2018; Wang et al. 2019), whereas CcmM58 has an N-terminal γ-CA-like domain that has been suggested to interact with β-CA (Pena et al. 2010; Zang et al. 2021), in addition to 3 C-terminal SSUL domains. Both CcmM35 and CcmM58 accounted for 6% of the total molecular mass. Interestingly, the shell–cargo complex linker protein, CcmN, exhibited a very low abundance, accounting for only 0.02% of the total molecular mass, and was not present in a specific stoichiometric ratio to CcmM58.

Discussion

Carboxysomes are natural organelle-like microcompartments responsible for CO_2 fixation in cyanobacteria and some proteobacteria, which serve as important players in the global carbon cycle. Due to their self-assembly, encapsulation, and selective permeability properties that facilitate efficient CO_2 fixation, carboxysomes have attracted considerable interest in basic research and bioengineering applications. In this study, we performed

Table 1. Protein stoichiometry of Syn7942 β-carboxysome determined by QconCAT

Category	Protein	Structure of functional unit	Molecular mass	% of total protein	Units of monomers per carboxysome	Functional units of multimer per carboxysome
Structural proteins	CcmK2	Hexamer (PDB: 4OX7) (Cai et al. 2015)	10.9 kDa	24.3 ± 2.6	11,853 ± 2191	1,975 ± 365
	CcmK3	Hexamer[a]	10.8 kDa	0.03 ± 0.01	12 ± 2	2 ± 0
	CcmK4	Hexamer (PDB: 4OX6) (Cai et al. 2015)	11.9 kDa	0.29 ± 0.05	127 ± 27	21 ± 4
	CcmL	Pentamer (PDB: 2QW7) (Tanaka et al. 2008)	11.0 kDa	0.07 ± 0.02	29 ± 8	6 ± 2
	CcmO	Pseudohexamer[a]	29.4 kDa	0.04 ± 0.05	7 ± 7	1 ± 1
	CcmP	Pseudohexamer (PDB: 5LSR) (Larsson et al. 2017)	23.2 kDa	0.14 ± 0.12	30 ± 22	5 ± 4
	CcmM35	Monomer	35.2 kDa	4.8 ± 1.8	730 ± 331	730 ± 331
	CcmM58	Monomer	57.8 kDa	1.22 ± 0.21	112 ± 27	112 ± 27
	CcmN	Monomer	16.3 kDa	0.03 ± 0.01	8 ± 2	8 ± 2
Catalytic proteins	RbcL	L_8S_8 hexadecamer (PDB: 1RBL) (Newman et al. 1993)	52.4 kDa	50.9 ± 4.9	5,112	639
	RbcS	L_8S_8 hexadecamer (PDB: 1RBL) (Newman et al. 1993)	13.3 kDa	17.4 ± 1	6,919 ± 825	865 ± 103
	RbcX	Dimer (PDB: 2PY8) (Tanaka et al. 2007)	17.0 kDa	0.03 ± 0.03	7 ± 7	3 ± 4
	CcaA	Hexamer (PDB: 5SWC) (McGurn et al. 2016)	30.2 kDa	0.93 ± 0.76	169 ± 151	28 ± 25
Intact β-carboxysome			529.4 MDa			

[a]Based on the sequence homology of CcmK3 and CcmK4, and of CcmO and CcmP. Data are presented as means ± SD from 4 independent biological replicates.

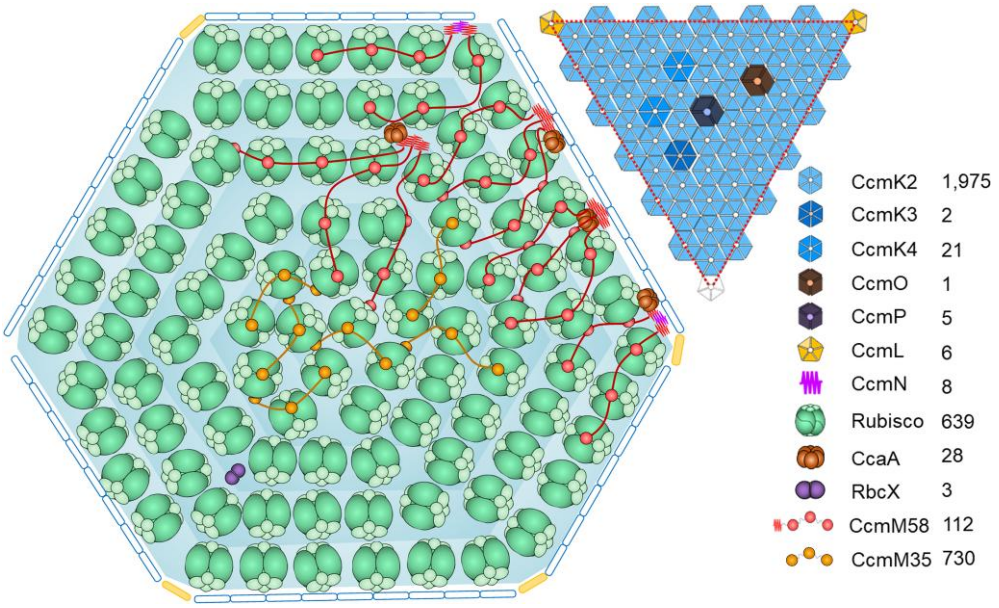

Figure 5. Schematic model of the Syn7942 β-carboxysome structure. The model illustrates the interior organization and shell facet composition determined by QconCAT-determined stoichiometry and cryoET. Rubiscos (green) are organized in multiple layers in the carboxysome. CcmN (fuchsia) and the N-terminus of CcmM58 (red fragment) mediate the Rubisco-shell binding. Rubiscos are crosslinked by SSUL of CcmM58 (red) and CcmM35 (orange). CcaA (brown) and RbcX (purple) are co-encapsulated with the Rubisco matrix. On the shell, CcmK3, CcmK4, CcmO, and CcmP are integrated into the facets formed predominantly by CcmK2 hexamers. The vertexes are partially capped by CcmL pentamers. The numbers of proteins present in the model are for illustration purposes only and do not correlate to actual abundances, which are displayed separately on the right.

cryoET analysis and absolute quantification using QconCAT-based LC-MS to determine Rubisco packaging and stoichiometric composition of functional, intact Syn7942 β-carboxysomes, a model system widely used in carboxysome studies.

Based on our findings, we propose a model of the entire β-carboxysome structure from Syn7942 (Fig. 5). CcmK2 hexamers are the dominant components of the β-carboxysome shell. Other shell proteins, including the CcmK4 and CcmK3 hexamers and the CcmO and CcmP pseudo-hexamers, tile the shell facets. On average, only 6 copies of CcmL pentamers were found per β-carboxysome, which is comparable to the examined CcmL content per β-carboxysome using fluorescence imaging quantification (Sun et al. 2019). It is less than both the theoretical estimation of 12 pentagons per canonical icosahedron and the determined number of CsoS4 pentamers (11 copies) per α-carboxysome (Sun et al. 2022). This discrepancy suggests an increased likelihood of incomplete

capping at the vertices of β-carboxysomes and likely leads to the greater structural variability of β-carboxysomes compared to that of α-carboxysomes. More than 600 Rubisco L_8S_8 hexadecamers were encapsulated within the Syn7942 β-carboxysome with a diameter of 170 nm. Rubiscos are organized in several concentric layers parallel to the outer shell, with Rubisco complexes oriented predominantly in the radial direction (Supplementary Fig. S4). The CcmN–CcmM assemblies play an essential role in bridging the association between the shell and cargo enzymes. Our results suggest that there are, on average, 8 copies of CcmN in each β-carboxysome, in contrast to 112 copies of CcmM58 and 730 copies of CcmM35. This is strikingly distinct from the previously estimated CcmN:CcmM stoichiometry based on in vitro studies (Sun et al. 2021). Moreover, both our findings and previous structural analysis of reconstituted Rubisco–CcmM complexes (Wang et al. 2019) reveal that the SSUL modules of CcmM58 and CcmM35 bind Rubiscos and crosslink neighboring Rubiscos, mediating Rubisco recruitment and packaging within the β-carboxysome. CcmM58 and CcmM35 may crosslink multiple Rubiscos within the same layer or across different layers. Although each Rubisco has 4 CcmM SSUL-binding sites, our data suggest that the SSUL domains have low occupancy on individual Rubiscos (Fig. 2F), which might provide the foundation for the formation of Rubisco condensates and their organizational flexibility. Additionally, there are 28 CcaA enzymes and 3 RbcX proteins encapsulated within the β-carboxysome lumen, which are essential for the assembly and carboxylation activity of Rubiscos.

This specific Rubisco organization identified may provide the foundation for packaging the maximum number of Rubisco complexes into the limited internal space of the β-carboxysome. This dense packing and concentration of Rubisco is thought to enhance carboxylation reactions of each individual β-carboxysome and help the cell make the most of its available space and resources to maximize its CO_2-fixing capacity. Moreover, our previous studies have revealed a notable size variation of β-carboxysomes in Syn7942 (ranging from 144 to 208 nm) under various environmental conditions, such as light intensity and CO_2 availability; larger β-carboxysomes can accommodate more Rubisco complexes, with 367 copies of Rubiscos within the β-carboxysome of 144 nm in diameter compared to 1,507 Rubiscos within a 208 nm-diameter β-carboxysome (Sun et al. 2019). The present work and recent studies (Kong et al. 2024) on Syn7942 β-carboxysomes using cryoET further verified this structural variation. Within a β-carboxysome with a diameter of 169 nm, ~640 Rubisco enzymes were organized into 5 concentric layers (Fig. 2). A larger β-carboxysome with a size of 193 nm can accommodate an additional Rubisco layer arranged close to the shell, due to the 12 nm distances between neighboring Rubiscos (Supplementary Fig. S3), allowing for over 400 additional Rubiscos and more than 1,200 Rubisco enzymes in total encapsulated within the larger β-carboxysome structure (Kong et al. 2024). The carboxysome diameter, as well as the abundance and packing of interior Rubisco, is important factors in determining the overall architecture and physical mechanics of the intact β-carboxysome (Faulkner et al. 2017). These findings underscore the organizational and functional dynamics and flexibility of native β-carboxysomes, a possible mechanism for their adaptation in response to environmental changes. How specific Rubisco packaging is established within the carboxysome and how it determines precisely the carboxysome functionality and the physiological adaptation of cyanobacterial cells in response to environmental changes remain to be explored.

The findings on β-carboxysomes and α-carboxysomes allow extensive comparisons of the structures and assembly mechanisms of the 2 distinct carboxysome linkages, although the smaller Syn7942 β-carboxysomes characterized in this study were still larger than the previously reported α-carboxysomes. Recently studies have suggested that the middle region of CsoS2 plays a crucial role in determining the size of the α-carboxysome (Li et al. 2024; Oltrogge et al. 2024). In contrast, what determines the size of β-carboxysomes remains unclear. Our results imply that the composition of scaffolding proteins may drive variations in carboxysome diameter. The ratio of short to long isoforms of CcmM is nearly 5 times that of CsoS2 (Supplementary Table S4), which presumably favors cargo packaging rather than cargo–shell interactions in the β-carboxysome (Long et al. 2010; Kinney et al. 2012; Wang et al. 2019; Sun et al. 2021; Zang et al. 2021), resulting in the formation of a large cargo core. In contrast, CcmN, the linker protein that binds directly with shell proteins, has a relatively low abundance (Table 1), suggesting that CcmN is unlikely to be the key factor in determining β-carboxysome size. Nevertheless, despite the difference in the size of the 2 types of carboxysomes, the ratios between the shell proteins and cargo enzymes remained consistent (Supplementary Table S4), which may be fundamental for maintaining complete encapsulation and overall polyhedral architecture. Although Rubisco packaging and CcmM binding have been identified, how low-abundance proteins, such as CcmN and β-CA, are integrated within the β-carboxysome remains unclear.

It has been proposed that α- and β-carboxysomes exploit different assembly pathways. *De novo* assembly of β-carboxysomes exploits the "Core first" mode, in which Rubiscos are first condensed, mediated by CcmM, to form a liquid-like Rubisco matrix core, followed by shell encapsulation (Cameron et al. 2013; Chen et al. 2013). In contrast, the construction of the Rubisco core and shell encapsulation during α-carboxysome assembly, mediated by CsoS2, is assumed to occur in a simultaneous and/or separate fashion (Iancu et al. 2010). The cryoET data by us and others revealed that Rubiscos within Syn7942 β-carboxysomes form multiple concentric layers parallel to the shell, which share a similar organizational pattern as Rubiscos in α-carboxysomes from *Cyanobium* and *Prochlorococcus* but are distinct from the Rubisco packaging in *H. neap* α-carboxysomes (Ni et al. 2022a, 2022b; Evans et al. 2023; Kong et al. 2024; Zhou et al. 2024). While the β-carboxysome structures differ in their 3D shape and quantity of concentric layers, our data revealed that there are no significant differences observed in the arrangement and orientation of Rubiscos within each concentric layer among different layers in Syn7942 β-carboxysomes (Fig. 2, Supplementary Fig. S4). In addition, the ratios of Rubisco to scaffolding proteins CcmM/CsoS2 in Syn7942 and *H. neap* carboxysomes remained relatively consistent. Overall, the remarkable structural variations in carboxysomes from different native host organisms highlight their modular features and reprogrammable potential, which may be vital for microorganisms to adapt carboxysome functions and CO_2 assimilation to specific ecological niches (Sun et al. 2016, 2019; Nguyen et al. 2024). Our results also suggest that evaluating the architecture of mature carboxysomes alone does not provide a definitive way to differentiate between the distinct assembly mechanisms of α- and β-carboxysomes.

In summary, this study highlights the assembly principles and inherent structural variability of β-carboxysomes, which enables a better understanding of their structural plasticity and functional regulation and facilitates the engineering and reprogramming of carboxysomes for new functions.

Materials and methods

Bacterial strains, growth conditions, and carboxysome production

S. elongatus PCC 7942 (Syn7942) cells were cultivated in BG-11 medium (Rippka et al. 1979) or BG-11 agar plates with TES (N-tris(hydroxymethyl)methyl-2-aminoethanesulfonic acid) buffer pH 8.2 (22.9% w/w of $C_6H_{15}NO_6S$) and sodium thiosulfate (0.3% w/w of $Na_2S_2O_3$), solidified on 1.5% agar (w/v). Syn7942 cells were maintained in 5-L Duran flasks under constant low-light illumination (15 $\mu E\ m^{-2}\ s^{-1}$, measured at the culture surface) with aeration and agitation, which enable the production of β-carboxysomes with a smaller diameter (Faulkner et al. 2017; Sun et al. 2019).

Carboxysome purification from Syn7942

The β-carboxysome purification was performed as previously described with some modifications (Sun et al. 2016; Faulkner et al. 2017). Syn7942 cells from a 16-L culture were harvested at the late-exponential phase when OD_{750} reached 1.5 to 2. The cell pellet was resuspended and incubated in TE buffer (20 mM Tris–HCl pH 8.0, 0.5 mM EDTA) in the presence of 2% cell lytic B (Sigma Aldrich, USA), 1% protease inhibitor cocktails (Thermo Fisher, UK) and 0.5 mg mL^{-1} lysozyme (Sigma Aldrich) for 1 h prior to cell breakage by glass beads beating. Lysates were incubated overnight with 1% Triton X-100 and 0.5% IGPAL CA-630 for membrane solubilization. Lysates were briefly centrifuged at 3,000 × *g* to remove large debris, and the supernatant was centrifuged at 40,000 × *g* for 1 h to obtain crude β-carboxysome enrichment. The crude enrichments were further treated with 1% *n*-dodecyl-β-D-maltoside and 1% DNase for 2 h and then loaded on an identical step sucrose gradient centrifugation used for recombinant β-carboxysomes. Enriched β-carboxysomes were collected from the 50% to 60% sucrose gradient fractions.

SDS–PAGE and immunoblot analysis

SDS–PAGE was performed following standard procedures. About 5 to 10 μg purified carboxysome proteins were loaded per well on 15% polyacrylamide gels and stained with Coomassie Brilliant Blue G-250 (Thermo Fisher Scientific, UK). The sizes of the protein bands were referenced to the PageRuler Plus Prestained Protein Ladder (Thermo Fisher Scientific). Immunoblot analysis was performed using primary rabbit polyclonal anti-RbcL (1:10,000 dilution, AS03 037, Agrisera), rabbit polyclonal anti-CcmK2 (1:5,000 dilution, PHY5336S, Phytoab), working with secondary antibody anti-rabbit IgG secondary antibody (1:10,000 dilution, Agrisera), and horseradish peroxidase-conjugated goat anti-mouse IgG secondary antibody (1:10,000 dilution, Agrisera). Images were acquired using the Quant LAS 4000 platform (GE Healthcare Life Sciences). Quantification of band intensities was performed using ImageJ software.

Rubisco activity assays

$^{14}CO_2$ fixation assay was performed to determine the CO_2-fixation rate of purified β-carboxysomes, as described previously (Sun et al. 2016). Three independently purified carboxysomes were calibrated to 0.2 mg mL^{-1} and added Rubisco assay buffer (100 mm EPPS, pH 8.0, and 20 mm $MgCl_2$) at 0.1 μg, assayed was performed at 30 °C and initiated with the final concentration of 0.5 mM RuBP. The concentration of HCO_3 was set to 24 mM for all assays in this study.

Electron microscopy and data analysis

Electron microscopy was performed as previously described (Faulkner et al. 2017; Huang et al. 2020; Chen et al. 2022; Sun et al. 2022). The purified carboxysomes (~2 mg mL^{-1}) were stained with 3% uranyl acetate on carbon grids and then inspected using an FEI (Field Electron and Ion Company) 120 kV Tecnai G2 Spirit BioTWIN TEM equipped with a Gatan Rio 16 Camera. The diameters of carboxysomes were measured using ImageJ as described previously (Faulkner et al. 2017; Sun et al. 2022).

CryoET sample preparation, data acquisition, and data analysis

To prepare the cryoET grids for β-carboxysomes, 500 μL purified β-carboxysomes in 60% sucrose were diluted to 5 mL with TEMB buffer (10 mM Tris-HCl, pH 8.0, 1 mM EDTA, 10 mM $MgCl_2$, 20 mM $NaHCO_3$) and concentrated to 100 μL using 100 K centrifugal filters (Amicon Ultra) by centrifugation at 700 × *g* for 10 min to remove sucrose. Then, 100 μL β-carboxysomes were diluted to 5 mL again and concentrated to a final volume of 50 μL (10× concentrated with 0.6% sucrose in TEMB buffer). The concentrated β-carboxysomes were plunge-frozen in ethane onto lacey holy carbon grids (300 mesh, Agar Scientific) using a Leica GP2. The grids were glow-discharged for 45 s before plunge freezing, and gold fiducial beads (7 nm) were mixed with the sample before sample application to the grids. The excess solution was blotted for 3 or 3.5 s with a humidity of 100% and a temperature of 20 °C.

Optimized cryoET grids were loaded onto a Titan Krios microscope (Thermo Fisher Scientific) operated at 300 keV in the Electron Bio-Imaging Centre, Diamond. The dataset was acquired using a Gatan Quantum post-column energy filter (Gatan Inc.) operated in zero-loss mode with a 20-eV slit width, paired with a Gatan K3 direct electron detector, using Thermo Scientific Tomography 5 Software by electron counting in super-resolution mode at a physical pixel size of 1.35 per pixel. The tilt series was collected using a dose-symmetric tilt scheme starting from 0 ° with a 3 ° tilt increment by a group of 3 and an angular range of ±60 °. The accumulated dose of each tilt series was around 120 $e^-/Å^2$ with a defocus range between −2.5 and −5.5 μm. Ten raw frames were saved for each tilt series. The details of the data collection process are presented in Supplementary Table S1.

For cryoET data analysis, the tilt series for β-carboxysomes were aligned with IMOD (v4.9.12) (Kremer et al. 1996) using gold fiducials, with the aid of an in-house on-the-fly processing Python script (https://github.com/ffyr2w/cet_toolbox). The center of each identified gold fiducial was checked manually. STA was performed using emClarity (v1.5.0.4, v1.6.2) (Ni et al. 2022a, 2022b). The Rubisco crystal structure (PDB ID: 5NV3) was converted to a density map at 20 Å resolution with a molmap command in Chimera and then used as the template for particle searching using emClarity. Template matching was performed using 4× binned tomograms with a pixel size of 5.4 Å (hereafter bin4 tomograms). Rubisco coordinates were manually checked using IMOD to remove false positives and individual Rubiscos outside the β-carboxysome. A total of 185 β-carboxysomes were used for STA and alignment. The averaging and alignment were first performed at bin3 with a pixel size of 4.05 Å for 4 cycles, followed by bin2 with a pixel size of 2.70 Å pixel for 8 cycles, and bin1 with a pixel size of 1.35 Å for 4 cycles. The dataset was divided into 2 independent subsets during alignment for gold-standard metrics, and the 2 subsets were combined in the final iteration, resulting in a final resolution of 3.7 Å. D4 symmetry was applied throughout the alignment procedure and the final density map was reconstructed using 2D tilt series images with cisTEM

within the emClarity package at a resolution of 3.5 Å. As for the radial and angular distribution of Rubiscos, the core of each β-carboxysomes was defined as the average of all Rubiscos positions within the β-carboxysome. The distance between each refined Rubisco and the β-carboxysome core was generated to plot the radial distance distribution. A radial vector for each Rubisco was calculated pointing from the core of its corresponding β-carboxysomes to each Rubisco, while the angle between the radial vector and the 4-fold axis or Rubisco was generated to investigate the radial angular distribution.

CryoET of Syn7942 cells was performed as previously described (Huokko et al. 2021). For cell vitrification and cryo-focused ion beam (cryo-FIB) milling, Syn7942 cells were diluted to OD_{750} = ~0.8 in their culture medium before plunge freezing. Three microliters of suspended cells in a culture medium was applied to the front side of glow-discharged R2/2 carbon-coated copper grids (Quantifoil MicroTools), with additional 1 μL cells added to the backside. The grids were blotted for 4 s before being vitrified in liquid ethane using a Leica GP2 plunge freezer. The vitrified grids were subsequently loaded onto an Aquilos FIB/scanning electron microscope (FIB/SEM) (Thermo Fisher Scientific) to prepare thin lamellae of the cells. To reduce overall specimen charging, the grids were sputter-coated with platinum before milling. The ion beam current was gradually adjusted to lower values as the lamellae thinning progressed (first using 0.1 nA until 0.75 μm thick, and then 50 pA until ~250 nm thick). For cryoET data collection, tomography tilt series were acquired from lamella using a Titan Krios microscope (Thermo Fisher Scientific) operated at 300 kV. The tilt series data were acquired with a stage pretilt of −7 ° to account for the angle of lamella, making the lamella surface roughly perpendicular to the electron beam. Tilt series were collected from −42 to 42 ° in 2° increment by a group of 3 using a dose-symmetric scheme (Hagen et al. 2017) in SerialEM (Mastronarde 2005), with a target defocus of −10 μm. The tilt series reconstruction was performed with a binning factor of 4, resulting in a final pixel size of 2.492 nm. Micrographs were recorded with a K3 camera equipped with a Gatan Quantum energy filter operated in zero-loss mode with a 20 eV slit width. The exposure time was set to 5 s, and the videos were fractionated into 10 subframes. The nominal magnification of the recorded images was 15,000×, with a pixel size of 6.23 Å. The total accumulated dose was ~120 $e^{-}/Å^{2}$.

Design, cell-free expression, and purification of QconCAT standard

Absolute quantification of carboxysome protein components was performed using concatenated signature QconCAT peptides (Pratt et al. 2006) in a manner similar to that described previously (Yang et al. 2020; Sun et al. 2022). Briefly, 2 qualified peptide candidates were selected to quantify each protein. Candidate peptides were BLAST searched against the protein database in the Syn7942 database to ensure their uniqueness. The DNA fragment encoding the above peptides, together with GluFib and cMyc, as well as 6× His-tag at the N-terminus and C-terminus, respectively, were generated following the ALACAT/Qbrick assembly strategy, as reported previously (Johnson et al. 2021). The final DNA sequence (Supplementary Table S2) was assembled into a pEU-E01 vector for cell-free expression using wheat germ cell lysates (CellFree Sciences Co. Ltd, Japan). Synthesis was completed with [$^{13}C_6$, $^{15}N_4$] arginine and [$^{13}C_6$, $^{15}N_2$] lysine (CK Isotopes Ltd, UK) using a WEPR8240H full Expression kit following default protocols (2BScientific Ltd, UK). The QconCAT peptides were purified using a HisTrap HP Column (Cytiva, UK) following standard methods. The QconCAT was precipitated and resuspended in 30 μL 25 mM ammonium bicarbonate with 0.1% (w/v) RapiGest SF surfactant (Waters, UK) and protease inhibitors (Roche cOmplete, Mini, EDTA-free Protease Inhibitor Cocktail, Merck, UK).

Proteomic analysis

Proteomic analysis was performed on 4 independent biological replicates as previously described with modifications (Sun et al. 2022). Designed QconCAT Peptides for β-carboxysome protein quantification were listed in Supplementary Table S2. The overall protein and DNA sequence of QconCAT were provided in Supplementary Table S3. For sample handling, the protein concentration of each sample was determined using a NanoDrop Spectrophotometer (Thermo Fisher Scientific). Carboxysome samples were diluted to a final protein concentration of 2 μg per 72 μL of 50 mM NH_4HCO_3. QconCAT (~0.6 pmol), and the samples were denatured using 8 μL of 10% (w/v) SDS (Thermo Fisher Scientific) in 50 mM NH_4HCO_3 followed by incubation at 80 °C for 10 min. Samples were reduced by the addition of 5 μL 12 mM dithiothreitol in 50 mM NH_4HCO_3 and incubated at 60 °C for 10 min. Alkylation was carried out by adding 5 μL of 36 mM iodoacetamide in 50 mM NH_4HCO_3 and incubation at room temperature for 30 min in the dark. The treated samples were then bound to 40 ng of SP3 Beads (Cytiva, UK) by the addition of acetonitrile to a final concentration of 80% acetonitrile and incubated for 30 min. The beads were washed 3 times with 100% acetonitrile and once with 100% water. The beads were resuspended in 50 mM NH_4HCO_3 and the sample was digested with trypsin (1 μL of 200 ng in 50 mM NH_4HCO_3 in a final volume of 20 μL). Samples were incubated at 37 °C overnight, followed by centrifugation at 17,200 × *g* for 30 min, and transferred to fresh low-binding tubes. Three biological replicates were analyzed using an UltiMate 3000 RSLCnano system coupled to a Q Exactive HF Hybrid Quadrupole-Orbitrap Mass Spectrometer (Thermo Fisher Scientific) in data-dependent acquisition mode, according to a previously published protocol (Johnson et al. 2021). The LC was operated under the control of Dionex Chromatography MS Link 2.14. The raw MS data files were loaded into Thermo Proteome Discoverer v.2.4 (Thermo Fisher Scientific) and searched against the carboxysome QconCAT database using Mascot v.2.8 (Matrix Science London, UK) with trypsin as the specified enzyme. Each precursor ion was cleanly isolated at the high-resolution scanning speed of the MS1 approach. A precursor mass tolerance of 10 ppm and a fragment ion mass tolerance of 0.01 Da were applied. Data analysis, including run alignment and peak picking, was carried out using Skyline v23.1 (MacCoss Lab Software) (MacLean et al. 2010; Pino et al. 2020). Single carboxysome quantitative normalization was performed using Rubisco counts measured from cryoET, as shown in Fig. 2C.

Statistical analyses

Data are presented as means and SD determined from multiple independent biological replicates as specified by *n* for individual experiments. Statistical analysis was conducted using Origin (OriginLab, Massachusetts, USA); statistical significance was determined by Student's *t*-test.

Accession numbers

Sequence data from this article can be found in the GenBank/EMBL data libraries under accession numbers AAA27304.1 (CcmK2), ABB56316.1 (CcmK3), ABB56317.1 (CcmK4), AAA27305.1 (CcmL), AAA27306.1 (CcmM), AAA27326.1 (CcmN), AAA27327.1 (CcmO), ABB56552.1 (CcmP), ABB57456.1 (RbcL), ABB57457.1 (RbcS), ABB57565.1 (RbcX), and AAA27315.1 (CcaA).

Acknowledgments

We thank the staff at the Liverpool Biomedical Electron Microscopy unit for their support with negative-staining electron microscopy. Computation was performed at the Diamond Light Source and the Oxford Biomedical Research Computing (BMRC) facility, a joint development between the Wellcome Centre for Human Genetics and the Big Data Institute (BDI) supported by the Health Data Research UK and the NIHR Oxford Biomedical Research Centre.

Author contributions

Ya.S., P.Z., and L-N.L. conceived the project. Ya.S. and X.G. performed carboxysome preparation and biochemical characterization. J.S., P.J.B., Ya.S., N.R., and C.E.E. conducted MS and data analysis. G.F.D. performed negative-staining EM. Yu.S. and T.N. collected cryoET datasets, processed cryoET data, and subtomogram averaging. K.L. and N.H. refined Rubisco structures. T.N. performed cryo-FIB/SEM lamella preparation, cryoET data collection, and reconstruction. Yu.S., T.N., P.Z., and L-N.L. analyzed the structural data. Ya.S, Yu.S, P.Z., and L-N.L. wrote the manuscript with contributions from all the authors.

Supplementary data

The following materials are available in the online version of this article.

Supplementary Figure S1. Isolation and identification of Syn7942 β-carboxysomes.

Supplementary Figure S2. Positioning of Rubiscos in a β-carboxysome by template matching using emClarity.

Supplementary Figure S3. Layer profiles of Rubiscos within β-carboxysomes.

Supplementary Figure S4. Orientation profile of Rubiscos within β-carboxysomes.

Supplementary Figure S5. The density and fittings of the Rubisco small subunit-like (SSUL) domain of CcmM on Rubisco.

Supplementary Figure S6. Design and preparation of Quantification conCATamer (QconCAT) quantification.

Supplementary Table S1. CryoET data collection, processing and model refinement statistics.

Supplementary Table S2. QconCAT peptides derived from tryptic proteolysis for β-carboxysome protein quantification.

Supplementary Table S3. DNA and protein sequences of the β-carboxysome QconCAT peptide.

Supplementary Table S4. Comparison of the protein ratios of β-carboxysomes from Syn7942 and α-carboxysomes from *H. neapolitanus*.

Supplementary Video S1. Template matching results show the Rubisco packaging and the spatial positions of matched Rubiscos within the β-carboxysome.

Supplementary Video S2. Structure of Rubisco from β-carboxysomes by cryoET subtomogram averaging.

Supplementary Video S3. Binding of CcmM SSUL to Rubisco within the β-carboxysome determined by cryoET subtomogram averaging.

Supplementary Video S4. Tomographic slices view of Syn7942 cell lamella.

Supplementary Data Set 1. QconCAT data of β-carboxysome proteins within the isolated Syn7942.

Funding

This work was supported by the National Key Research and Development Program of China (2023YFA0914600 and 2021YFA0909600), National Natural Science Foundation of China (32070109), Biotechnology and Biological Sciences Research Council Grant (BB/Y01135X/1, BB/V009729/1, and BB/S003339/1), Leverhulme Trust (RPG-2021-286 and RPG-2019-300), Natural Environment Research Council Grant (NE/Z00019X/1), Royal Society (URF\R\180030 and RGF\EA\181061), European Research Council (ERC) Advanced Grant (101021133), National Institutes of Health (P50AI150481), and Wellcome Trust Investigator Award (206422/Z/17/Z). We thank Diamond Light source for access and support of the cryoEM facilities at the UK National Electron Bio-Imaging Centre [eBIC (proposal NT21004)], funded by the Wellcome Trust, Medical Research Council, and BBSRC.

Conflict of interest statement. The authors declare no conflict of interest.

Data availability

All data needed to evaluate the conclusions are presented in the paper and/or in Supplementary information. The cryoET subtomogram averaging density maps and corresponding atomic models were deposited in the PDB and EMDB, with accession codes 9FWV (https://doi.org/10.2210/pdb9FWV/pdb) and EMD-50836 (https://www.ebi.ac.uk/emdb/EMD-50836), respectively.

References

Behrenfeld MJ, Randerson JT, McClain CR, Feldman GC, Los SO, Tucker CJ, Falkowski PG, Field CB, Frouin R, Esaias WE, *et al.* Biospheric primary production during an ENSO transition. *Science*. 2001: 291(5513):2594–2597. https://doi.org/10.1126/science.1055071

Cai F, Sutter M, Bernstein SL, Kinney JN, Kerfeld CA. Engineering bacterial microcompartment shells: chimeric shell proteins and chimeric carboxysome shells. *ACS Synth Biol*. 2015:4(4):444–453. https://doi.org/10.1021/sb500226j

Cai F, Sutter M, Cameron JC, Stanley DN, Kinney JN, Kerfeld CA. The structure of CcmP, a tandem bacterial microcompartment domain protein from the β-carboxysome, forms a subcompartment within a microcompartment. *J Biol Chem*. 2013:288(22): 16055–16063. https://doi.org/10.1074/jbc.M113.456897

Cameron JC, Wilson SC, Bernstein SL, Kerfeld CA. Biogenesis of a bacterial organelle: the carboxysome assembly pathway. *Cell*. 2013:155(5):1131–1140. https://doi.org/10.1016/j.cell.2013.10.044

Chen AH, Robinson-Mosher A, Savage DF, Silver PA, Polka JK. The bacterial carbon-fixing organelle is formed by shell envelopment of preassembled cargo. *PLoS One*. 2013:8(9):e76127. https://doi.org/10.1371/journal.pone.0076127

Chen T, Fang Y, Jiang Q, Dykes GF, Lin Y, Price GD, Long BM, Liu LN. Incorporation of functional Rubisco activases into engineered carboxysomes to enhance carbon fixation. *ACS Synth Biol*. 2022:11(1):154–161. https://doi.org/10.1021/acssynbio.1c00311

Chen X, Zheng F, Wang P, Mi H. Novel protein CcmS is required for stabilization of the assembly of β-carboxysome in *Synechocystis* sp. strain PCC 6803. *New Phytol*. 2023:239(4):1266–1280. https://doi.org/10.1111/nph.19016

Cheng J, Li C-Y, Meng M, Li J-X, Liu S-J, Cao H-Y, Wang N, Zhang Y-Z, Liu L-N. Molecular interactions of the chaperone CcmS and carboxysome shell protein CcmK1 that mediate β-carboxysome

assembly. *Plant Physiol*. 2024:196(3):1778–1787. https://doi.org/10.1093/plphys/kiae438

Cot SS, So AK, Espie GS. A multiprotein bicarbonate dehydration complex essential to carboxysome function in cyanobacteria. *J Bacteriol*. 2008:190(3):936–945. https://doi.org/10.1128/JB.01283-07

Eisenhut M, Aguirre von Wobeser E, Jonas L, Schubert H, Ibelings BW, Bauwe H, Matthijs HC, Hagemann M. Long-term response toward inorganic carbon limitation in wild type and glycolate turnover mutants of the cyanobacterium Synechocystis sp. strain PCC 6803. *Plant Physiol*. 2007:144(4):1946–1959. https://doi.org/10.1104/pp.107.103341

Evans SL, Al-Hazeem MMJ, Mann D, Smetacek N, Beavil AJ, Sun Y, Chen T, Dykes GF, Liu LN, Bergeron JRC. Single-particle cryo-EM analysis of the shell architecture and internal organization of an intact α-carboxysome. *Structure*. 2023:31(6):677–688.e4. https://doi.org/10.1016/j.str.2023.03.008

Faulkner M, Rodriguez-Ramos J, Dykes GF, Owen SV, Casella S, Simpson DM, Beynon RJ, Liu LN. Direct characterization of the native structure and mechanics of cyanobacterial carboxysomes. *Nanoscale*. 2017:9(30):10662–10673. https://doi.org/10.1039/C7NR02524F

Field CB, Behrenfeld MJ, Randerson JT, Falkowski P. Primary production of the biosphere: integrating terrestrial and oceanic components. *Science*. 1998:281(5374):237–240. https://doi.org/10.1126/science.281.5374.237

Gonzalez-Esquer CR, Newnham SE, Kerfeld CA. Bacterial microcompartments as metabolic modules for plant synthetic biology. *Plant J*. 2016:87(1):66–75. https://doi.org/10.1111/tpj.13166

Gonzalez-Esquer CR, Shubitowski TB, Kerfeld CA. Streamlined construction of the cyanobacterial CO_2-fixing organelle via protein domain fusions for use in plant synthetic biology. *Plant Cell*. 2015:27(9):2637–2644. https://doi.org/10.1105/tpc.15.00329

Hagen AR, Plegaria JS, Sloan N, Ferlez B, Aussignargues C, Burton R, Kerfeld CA. *In vitro* assembly of diverse bacterial microcompartment shell architectures. *Nano Lett*. 2018:18(11):7030–7037. https://doi.org/10.1021/acs.nanolett.8b02991

Hagen W, Wan W, Briggs J. Implementation of a cryo-electron tomography tilt-scheme optimized for high resolution subtomogram averaging. *J Struct Biol*. 2017:197(2):191–198. https://doi.org/10.1016/j.jsb.2016.06.007

Himes BA, Zhang P. emClarity: software for high-resolution cryo-electron tomography and subtomogram averaging. *Nat Methods*. 2018:15(11):955–961. https://doi.org/10.1038/s41592-018-0167-z

Huang F, Kong W, Sun Y, Chen T, Dykes GF, Jiang YL, Liu LN. Rubisco accumulation factor 1 (Raf1) plays essential roles in mediating Rubisco assembly and carboxysome biogenesis. *Proc Natl Acad Sci U S A*. 2020:117(29):17418–17428. https://doi.org/10.1073/pnas.2007990117

Huang F, Vasieva O, Sun Y, Faulkner M, Dykes GF, Zhao Z, Liu LN. Roles of RbcX in carboxysome biosynthesis in the cyanobacterium *Synechococcus elongatus* PCC7942. *Plant Physiol*. 2019:179(1):184–194. https://doi.org/10.1104/pp.18.01217

Huokko T, Ni T, Dykes GF, Simpson DM, Brownridge P, Conradi FD, Beynon RJ, Nixon PJ, Mullineaux CW, Zhang P, *et al*. Probing the biogenesis pathway and dynamics of thylakoid membranes. *Nat Commun*. 2021:12(1):3475. https://doi.org/10.1038/s41467-021-23680-1

Iancu CV, Morris DM, Dou Z, Heinhorst S, Cannon GC, Jensen GJ. Organization, structure, and assembly of alpha-carboxysomes determined by electron cryotomography of intact cells. *J Mol Biol*. 2010:396(1):105–117. https://doi.org/10.1016/j.jmb.2009.11.019

Johnson J, Harman VM, Franco C, Emmott E, Rockliffe N, Sun Y, Liu L-N, Takemori A, Takemori N, Beynon RJ. Construction of à la carte QconCAT protein standards for multiplexed quantification of user-specified target proteins. *BMC Biol*. 2021:19(1):195. https://doi.org/10.1186/s12915-021-01135-9

Kerfeld CA, Aussignargues C, Zarzycki J, Cai F, Sutter M. Bacterial microcompartments. *Nat Rev Microbiol*. 2018:16(5):277–290. https://doi.org/10.1038/nrmicro.2018.10

Kerfeld CA, Erbilgin O. Bacterial microcompartments and the modular construction of microbial metabolism. *Trends Microbiol*. 2015:23(1):22–34. https://doi.org/10.1016/j.tim.2014.10.003

Kerfeld CA, Melnicki MR. Assembly, function and evolution of cyanobacterial carboxysomes. *Curr Opin Plant Biol*. 2016:31:66–75. https://doi.org/10.1016/j.pbi.2016.03.009

Kerfeld CA, Sawaya MR, Tanaka S, Nguyen CV, Phillips M, Beeby M, Yeates TO. Protein structures forming the shell of primitive bacterial organelles. *Science*. 2005:309(5736):936–938. https://doi.org/10.1126/science.1113397

Kinney JN, Salmeen A, Cai F, Kerfeld CA. Elucidating essential role of conserved carboxysomal protein CcmN reveals common feature of bacterial microcompartment assembly. *J Biol Chem*. 2012:287(21):17729–17736. https://doi.org/10.1074/jbc.M112.355305

Kong WW, Zhu Y, Zhao HR, Du K, Zhou RQ, Li B, Yang F, Hou P, Huang XH, Chen Y, *et al*. Cryo-electron tomography reveals the packaging pattern of RuBisCOs in *Synechococcus* beta-carboxysome. *Structure*. 2024:32(8):1110–1120.e4. https://doi.org/10.1016/j.str.2024.05.007

Kremer JR, Mastronarde DN, McIntosh JR. Computer visualization of three-dimensional image data using IMOD. *J Struct Biol*. 1996:116(1):71–76. https://doi.org/10.1006/jsbi.1996.0013

Larsson AM, Hasse D, Valegård K, Andersson I. Crystal structures of β-carboxysome shell protein CcmP: ligand binding correlates with the closed or open central pore. *J Exp Bot*. 2017:68(14):3857–3867. https://doi.org/10.1093/jxb/erx070

Li T, Chen T, Chang P, Ge X, Chriscoli V, Dykes G, Wang Q, Liu L-N. Uncovering the roles of the scaffolding protein CsoS2 in mediating the assembly and shape of the α-carboxysome shell. *mBio*. 2024:15(10):e0135824. https://doi.org/10.1128/mbio.01358-24

Liu LN. Bacterial metabolosomes: new insights into their structure and bioengineering. *Microb Biotechnol*. 2021:14(1):88–93. https://doi.org/10.1111/1751-7915.13740

Liu LN. Advances in the bacterial organelles for CO_2 fixation. *Trends Microbiol*. 2022:30(6):567–580. https://doi.org/10.1016/j.tim.2021.10.004

Liu LN, Yang M, Sun Y, Yang J. Protein stoichiometry, structural plasticity and regulation of bacterial microcompartments. *Curr Opin Microbiol*. 2021:63:133–141. https://doi.org/10.1016/j.mib.2021.07.006

Long BM, Badger MR, Whitney SM, Price GD. Analysis of carboxysomes from Synechococcus PCC7942 reveals multiple Rubisco complexes with carboxysomal proteins CcmM and CcaA. *J Biol Chem*. 2007:282(40):29323–29335. https://doi.org/10.1074/jbc.M703896200

Long BM, Price GD, Badger MR. Proteomic assessment of an established technique for carboxysome enrichment from *Synechococcus* PCC7942. *Can J Bot*. 2005:83(7):746–757. https://doi.org/10.1139/b05-058

Long BM, Rae BD, Badger MR, Price GD. Over-expression of the beta-carboxysomal CcmM protein in Synechococcus PCC7942 reveals a tight co-regulation of carboxysomal carbonic anhydrase (CcaA) and M58 content. *Photosynth Res*. 2011:109(1–3):33–45. https://doi.org/10.1007/s11120-011-9659-8

Long BM, Rae BD, Rolland V, Förster B, Price GD. Cyanobacterial CO_2-concentrating mechanism components: function and prospects for plant metabolic engineering. *Curr Opin Plant Biol*. 2016:31:1–8. https://doi.org/10.1016/j.pbi.2016.03.002

Long BM, Tucker L, Badger MR, Price GD. Functional cyanobacterial β-carboxysomes have an absolute requirement for both long and short forms of the CcmM protein. *Plant Physiol*. 2010:153(1):285–293. https://doi.org/10.1104/pp.110.154948

MacLean B, Tomazela DM, Shulman N, Chambers M, Finney GL, Frewen B, Kern R, Tabb DL, Liebler DC, MacCoss MJ. Skyline: an open source document editor for creating and analyzing targeted proteomics experiments. *Bioinformatics*. 2010:26(7):966–968. https://doi.org/10.1093/bioinformatics/btq054

Mastronarde D. Automated electron microscope tomography using robust prediction of specimen movements. *J Struct Biol*. 2005:152(1):36–51. https://doi.org/10.1016/j.jsb.2005.07.007

McGrath JM, Long SP. Can the cyanobacterial carbon-concentrating mechanism increase photosynthesis in crop species? A theoretical analysis. *Plant Physiol*. 2014:164(4):2247–2261. https://doi.org/10.1104/pp.113.232611

McGurn LD, Moazami-Goudarzi M, White SA, Suwal T, Brar B, Tang JQ, Espie GS, Kimber MS. The structure, kinetics and interactions of the β-carboxysomal β-carbonic anhydrase, CcaA. *Biochem J*. 2016:473(24):4559–4572. https://doi.org/10.1042/BCJ20160773

Metskas LA, Ortega D, Oltrogge LM, Blikstad C, Lovejoy DR, Laughlin TG, Savage DF, Jensen GJ. Rubisco forms a lattice inside α-carboxysomes. *Nat Commun*. 2022:13(1):4863. https://doi.org/10.1038/s41467-022-32584-7

Newman J, Brändén CI, Jones TA. Structure determination and refinement of ribulose 1,5-bisphosphate carboxylase/oxygenase from Synechococcus PCC6301. *Acta Crystallogr D Biol Crystallogr*. 1993:49(6):548–560. https://doi.org/10.1107/S090744499300530X

Nguyen ND, Pulsford SB, Long BM. Unraveling Rubisco packaging within β-carboxysomes. *Structure*. 2024:32(8):1023–1025. https://doi.org/10.1016/j.str.2024.07.006

Ni T, Frosio T, Mendonça L, Sheng Y, Clare D, Himes BA, Zhang P. High-resolution in situ structure determination by cryo-electron tomography and subtomogram averaging using emClarity. *Nat Protoc*. 2022a:17(2):421–444. https://doi.org/10.1038/s41596-021-00648-5

Ni T, Jiang Q, Ng PC, Shen J, Dou H, Zhu Y, Radecke J, Dykes GF, Huang F, Liu L-N, *et al*. Intrinsically disordered CsoS2 acts as a general molecular thread for α-carboxysome shell assembly. *Nat Commun*. 2023:14(1):5512. https://doi.org/10.1038/s41467-023-41211-y

Ni T, Sun Y, Burn W, Al-Hazeem MMJ, Zhu Y, Yu X, Liu LN, Zhang P. Structure and assembly of cargo Rubisco in two native α-carboxysomes. *Nat Commun*. 2022b:13(1):4299. https://doi.org/10.1038/s41467-022-32004-w

Oltrogge LM, Chen AW, Chaijarasphong T, Turnšek JB, Savage DF. α-Carboxysome size is controlled by the disordered scaffold protein CsoS2. *Biochemistry*. 2024:63(2):219–229. https://doi.org/10.1021/acs.biochem.3c00403

Orr DJ, Worrall D, Lin MT, Carmo-Silva E, Hanson MR, Parry MAJ. Hybrid cyanobacterial-tobacco rubisco supports autotrophic growth and procarboxysomal aggregation. *Plant Physiol*. 2020:182(2):807–818. https://doi.org/10.1104/pp.19.01193

Peña KL, Castel SE, de Araujo C, Espie GS, Kimber MS. Structural basis of the oxidative activation of the carboxysomal gamma-carbonic anhydrase, CcmM. *Proc Natl Acad Sci U S A*. 2010:107(6):2455–2460. https://doi.org/10.1073/pnas.0910866107

Pino LK, Searle BC, Bollinger JG, Nunn B, MacLean B, MacCoss MJ. The skyline ecosystem: informatics for quantitative mass spectrometry proteomics. *Mass Spectrom Rev*. 2020:39(3):229–244. https://doi.org/10.1002/mas.21540

Pratt JM, Simpson DM, Doherty MK, Rivers J, Gaskell SJ, Beynon RJ. Multiplexed absolute quantification for proteomics using concatenated signature peptides encoded by QconCAT genes. *Nat Protoc*. 2006:1(2):1029–1043. https://doi.org/10.1038/nprot.2006.129

Price GD, Badger MR, Woodger FJ, Long BM. Advances in understanding the cyanobacterial CO_2-concentrating-mechanism (CCM): functional components, Ci transporters, diversity, genetic regulation and prospects for engineering into plants. *J Exp Bot*. 2008:59(7):1441–1461. https://doi.org/10.1093/jxb/erm112

Price GD, Pengelly JJ, Forster B, Du J, Whitney SM, von Caemmerer S, Badger MR, Howitt SM, Evans JR. The cyanobacterial CCM as a source of genes for improving photosynthetic CO2 fixation in crop species. *J Exp Bot*. 2013:64(3):753–768. https://doi.org/10.1093/jxb/ers257

Rae BD, Long BM, Badger MR, Price GD. Functions, compositions, and evolution of the two types of carboxysomes: polyhedral microcompartments that facilitate CO_2 fixation in cyanobacteria and some proteobacteria. *Microbiol Mol Biol Rev*. 2013:77(3):357–379. https://doi.org/10.1128/MMBR.00061-12

Rae BD, Long BM, Förster B, Nguyen ND, Velanis CN, Atkinson N, Hee WY, Mukherjee B, Price GD, McCormick AJ. Progress and challenges of engineering a biophysical CO_2-concentrating mechanism into higher plants. *J Exp Bot*. 2017:68(14):3717–3737. https://doi.org/10.1093/jxb/erx133

Rippka R, Deruelles J, Waterbury JB, Herdman M, Stanier RY. Generic assignments, strain histories and properties of pure cultures of Cyanobacteria. *Microbiology*. 1979:111(1):1–61. https://doi.org/10.1099/00221287-111-1-1

Rivers J, Simpson DM, Robertson DH, Gaskell SJ, Beynon RJ. Absolute multiplexed quantitative analysis of protein expression during muscle development using QconCAT. *Mol Cell Proteomics*. 2007:6(8):1416–1427. https://doi.org/10.1074/mcp.M600456-MCP200

Ryan P, Forrester TJB, Wroblewski C, Kenney TMG, Kitova EN, Klassen JS, Kimber MS. The small RbcS-like domains of the β-carboxysome structural protein CcmM bind RubisCO at a site distinct from that binding the RbcS subunit. *J Biol Chem*. 2019:294(8):2593–2603. https://doi.org/10.1074/jbc.RA118.006330

Savage DF, Afonso B, Chen AH, Silver PA. Spatially ordered dynamics of the bacterial carbon fixation machinery. *Science*. 2010:327(5970):1258–1261. https://doi.org/10.1126/science.1186090

Simpson DM, Beynon RJ. QconCATs: design and expression of concatenated protein standards for multiplexed protein quantification. *Anal Bioanal Chem*. 2012:404(4):977–989. https://doi.org/10.1007/s00216-012-6230-1

Sun H, Cui N, Han SJ, Chen ZP, Xia LY, Chen Y, Jiang YL, Zhou CZ. Complex structure reveals CcmM and CcmN form a heterotrimeric adaptor in β-carboxysome. *Protein Sci*. 2021:30(8):1566–1576. https://doi.org/10.1002/pro.4090

Sun Y, Casella S, Fang Y, Huang F, Faulkner M, Barrett S, Liu LN. Light modulates the biosynthesis and organization of cyanobacterial carbon fixation machinery through photosynthetic electron flow. *Plant Physiol*. 2016:171(1):530–541. https://doi.org/10.1104/pp.16.00107

Sun Y, Chen T, Ge X, Ni T, Dykes GF, Zhang P, Huang F, Liu LN. Engineering CO_2-fixing modules in *E. coli* via efficient assembly of cyanobacterial Rubisco and carboxysomes. *Plant Commun*. 2024:101217. https://doi.org/10.1016/j.xplc.2024.101217

Sun Y, Harman VM, Johnson JR, Brownridge PJ, Chen T, Dykes GF, Lin Y, Beynon RJ, Liu LN. Decoding the absolute stoichiometric composition and structural plasticity of α-carboxysomes. *mBio*. 2022:13(2):e0362921. https://doi.org/10.1128/mbio.03629-21

Sun Y, Wollman AJM, Huang F, Leake MC, Liu LN. Single-organelle quantification reveals the stoichiometric and structural variability of carboxysomes dependent on the environment. *Plant Cell*. 2019:31(7):1648–1664. https://doi.org/10.1105/tpc.18.00787

Takemori N, Takemori A, Tanaka Y, Endo Y, Hurst JL, Gomez-Baena G, Harman VM, Beynon RJ. MEERCAT: multiplexed efficient cell free expression of recombinant QconCATs for large scale absolute proteome quantification. *Mol Cell Proteomics*. 2017:16(12): 2169–2183. https://doi.org/10.1074/mcp.RA117.000284

Tanaka S, Kerfeld CA, Sawaya MR, Cai F, Heinhorst S, Cannon GC, Yeates TO. Atomic-level models of the bacterial carboxysome shell. *Science*. 2008:319(5866):1083–1086. https://doi.org/10.1126/science.1151458

Tanaka S, Sawaya MR, Kerfeld CA, Yeates TO. Structure of the RuBisCO chaperone RbcX from *Synechocystis* sp. PCC6803. *Acta Crystallogr D Biol Crystallogr*. 2007:63(10):1109–1112. https://doi.org/10.1107/S090744490704228X

Wang H, Yan X, Aigner H, Bracher A, Nguyen ND, Hee WY, Long BM, Price GD, Hartl FU, Hayer-Hartl M. Rubisco condensate formation by CcmM in β-carboxysome biogenesis. *Nature*. 2019:566(7742): 131–135. https://doi.org/10.1038/s41586-019-0880-5

Whitehead L, Long BM, Price GD, Badger MR. Comparing the *in vivo* function of α-carboxysomes and β-carboxysomes in two model cyanobacteria. *Plant Physiol*. 2014:165(1):398–411. https://doi.org/10.1104/pp.114.237941

Whitney SM, Houtz RL, Alonso H. Advancing our understanding and capacity to engineer nature's CO2-sequestering enzyme, Rubisco. *Plant Physiol*. 2011:155(1):27–35. https://doi.org/10.1104/pp.110.164814

Yang M, Simpson DM, Wenner N, Brownridge P, Harman VM, Hinton JCD, Beynon RJ, Liu LN. Decoding the stoichiometric composition and organisation of bacterial metabolosomes. *Nat Commun*. 2020:11(1):1976. https://doi.org/10.1038/s41467-020-15888-4

Zang K, Wang H, Hartl FU, Hayer-Hartl M. Scaffolding protein CcmM directs multiprotein phase separation in β-carboxysome biogenesis. *Nat Struct Mol Biol*. 2021:28(11):909–922. https://doi.org/10.1038/s41594-021-00676-5

Zhou R-Q, Jiang Y-L, Li H, Hou P, Kong W-W, Deng J-X, Chen Y, Zhou C-Z, Zeng Q. Structure and assembly of the α-carboxysome in the marine cyanobacterium *Prochlorococcus*. *Nat Plants*. 2024:10(4): 661–672. https://doi.org/10.1038/s41477-024-01660-9